DOI: 10.1002/chem.200901840

Understanding the Signatures of Secondary-Structure Elements in Proteins with Raman Optical Activity Spectroscopy

Christoph R. Jacob,* Sandra Luber, and Markus Reiher*[a]

Abstract: A prerequisite for the understanding of functional molecules like proteins is the elucidation of their structure under reaction conditions. Chiral vibrational spectroscopy is one option for this purpose, but provides only indirect access to this structural information. By first-principles calculations, we investigate how Raman optical activity (ROA) signals in proteins are generated and how signatures of specific secondary-structure elements arise. As a first target we focus on helical motifs and consider polypeptides consisting of twenty alanine residues to represent α-helical and 3_{10}-helical secondary-structure elements. Although ROA calculations on such large molecules have not been carried out before, our main goal is the stepwise reconstruction of the ROA signals. By analyzing the calculated ROA spectra in terms of rigorously defined localized vibrations, we investigate in detail how total band intensities and band shapes emerge. We find that the total band intensities can be understood in terms of the reconstructed localized vibrations on individual amino acid residues. Two different basic mechanisms determining the total band intensities can be established, and it is explained how structural changes affect the total band intensities. The band shapes can be rationalized in terms of the coupling between the localized vibrations on different residues, and we show how different band shapes arise as a consequence of different coupling patterns. As a result, it is demonstrated for the chiral variant of Raman spectroscopy how collective vibrations in proteins can be understood in terms of well-defined localized vibrations. Based on our calculations, we extract characteristic ROA signatures of α helices and of 3_{10}-helices, which our analysis directly relates to differences in secondary structure.

Keywords: ab initio calculations · chirality · helical structures · protein structures · vibrational spectroscopy

Introduction

To design molecules that perform a predefined function is one of the central goals of modern chemistry, ranging from materials science to nanotechnology, and from biochemistry to synthetic biology. A perfect example is the design of proteins that catalyze a given chemical reaction.[1,2] A prerequisite for such a design is, of course, the understanding of the relationship between protein structure and catalytic function. To study this relation, one needs experimental techniques that unambiguously identify structural elements in proteins while they are performing their catalytic task in their natural environment. Even though X-ray crystallography can be employed to obtain accurate protein structures with atomic resolution, it usually only provides static snapshots and cannot be applied in solution. Nuclear magnetic resonance (NMR) spectroscopy, on the other hand, can be used to obtain atomic-resolution protein structures in solution, but its time resolution is limited by the applied radiofrequency pulses to microseconds.[3] For this reason, NMR spectroscopy is not suited for studying fast structural changes (i.e., protein folding) or for investigating very flexible or disordered protein conformations. Therefore, complementary spectroscopic techniques are needed. One such alternative is provided by vibrational spectroscopy, which can be directly applied to proteins in solution and which potentially allows for femtosecond time resolution.[4,5]

However, conventional infrared (IR) and Raman spectra of polypeptides and proteins suffer from congested line shapes (i.e., they contain a large number of close-lying peaks that cannot be resolved experimentally).[6–8] Hence, vibrational spectroscopic techniques that either enhance the resolution by spreading out the spectroscopic information

[a] Dr. C. R. Jacob, S. Luber, Prof. Dr. M. Reiher
ETH Zurich, Laboratorium für Physikalische Chemie
Wolfgang-Pauli-Strasse 10, 8093 Zurich (Switzerland)
Fax: (+41) 44-63-31594
E-mail: markus.reiher@phys.chem.ethz.ch
christoph.jacob@phys.chem.ethz.ch

Supporting information for this article is available on the WWW under http://dx.doi.org/10.1002/chem.200901840.

over two frequency axes such as two-dimensional IR spectroscopy,[5,9–12] or that filter specific spectroscopic information such as resonance Raman spectroscopy[13–17] often provide more detailed information on the secondary structure of polypeptides and proteins. Similarly, chiral vibrational spectroscopy filters out information related to the chirality of the investigated molecule. Both the chiral variant of IR spectroscopy, vibrational circular dichroism (VCD),[18] and the chiral variant of Raman spectroscopy, Raman optical activity (ROA),[19–21] have been shown to be sensitive to peptide-backbone structure.

Due to this sensitivity, chiral vibrational spectroscopy is ideally suited for investigating the secondary structure of proteins in solution. Both VCD and ROA spectroscopy have been applied in many studies to gain information on the secondary structure of polypeptides and proteins.[22–27] As for nonchiral IR and Raman spectroscopy, these two techniques often provide complementary information. Here, we will focus on ROA spectroscopy, which has proven to provide information on the solution structure of polypeptides and proteins that in many cases is not accessible otherwise. For instance, it has been shown that ROA spectroscopy can be used to study the hydration state of α helices,[28] to discriminate different β-sheet structures,[29] and to study polypeptides and proteins adopting poly(L-proline) II (PPII) helical structures in solution.[30,31] Furthermore, it has been demonstrated that ROA spectroscopy can also be used to determine the absolute conformation of tryptophan side chains in proteins.[32,33]

However, even though a large number of ROA spectra of polypeptides and proteins have been recorded in the past decades, the understanding of the underlying mechanisms that determine these spectra remains rather incomplete. Therefore, the interpretation of measured ROA spectra of proteins and the assignment of certain spectral signatures to specific secondary-structure elements have mainly been based on the solution ROA spectra of certain proteins or model polypeptides for which the structure has been determined by X-ray crystallography (see, for example, ref. [24] and references therein) or on a careful comparison of different measured spectra, possibly using statistical techniques such as multivariate analysis methods.[34,35]

On the other hand, ab initio calculations of ROA spectra[36,37] allow us to predict the ROA spectrum for a given molecular structure from the first principles of quantum mechanics. By comparing the spectra calculated for several possible structures to the one observed experimentally, it is possible to determine which of the considered structures is present in the experiment. Such a procedure has been successful for small molecules, in particular for the assignment of absolute configurations.[38–40] For the interpretation of the ROA spectra of proteins and to identify signatures of secondary structure, one has to construct models of secondary-structure elements. However, realistic models require rather large polypeptides, and accurate ab initio calculations of ROA spectra for such systems are hampered by the large computational demands. For this reason, ROA calculations on realistic model systems have only become possible in recent years.[41] Alternatively, one can resort to more approximate methods,[42] in which results of calculations performed on smaller fragments are used to extrapolate to larger systems. A number of recent ROA studies of polypeptides and proteins have applied this approach to compare the measured spectra to the calculated spectra of models of different possible structures and thus to decide which secondary-structure elements are present in the experiment.[31,43]

However, ROA calculations for polypeptide model systems have so far only been used as a "fingerprint technique" (i.e., calculated spectra of different structural models have been compared to experimental data or to each other). Therefore, these studies have so far not led to detailed insight into the generation of the ROA signals in proteins. Such an understanding of the origin of ROA bands in proteins would make it possible to rationalize how structural changes affect the observed spectra and how spectral signatures of secondary-structure elements arise. This is also a prerequisite for developing reliable "rules of thumb" for the prediction of ROA spectra of proteins and would make it possible to develop simplified empirical models on the basis of parameters extracted from ab initio calculations on realistic model systems. In particular, one would like to know 1) which vibrations are responsible for the observed ROA bands; 2) what determines the signs and the intensities of these bands, and which groups of atoms are responsible for the observed ROA signals; and 3) what determines the observed band shapes, in particular whether a single peak, a couplet, or a more complicated band shape is found.

Besides the predicted ROA spectra, ab initio calculations also provide a wealth of additional information that is not available from experimental studies, such as the precise atomic displacements for each of the normal modes and the ROA intensities of each of them, which can further be divided into contributions of individual atoms or groups of atoms.[44] For small molecules, this information can be used to gain insight into the generation of ROA signals.[45–49] Although all this information is in principle directly available from the calculation for larger molecules as well as its interpretation is more difficult. The vibrational spectra of polypeptides and proteins consist of many bands with a large number of close-lying normal modes contributing to each band. However, these individual modes are usually not resolved in experiments. In ROA spectroscopy, the situation is further complicated by the fact that in many cases the individual modes contributing to one band show a rather irregular intensity pattern with positive and negative intensities for close-lying modes that may cancel each other out.[41] In addition, the normal modes are mostly delocalized over the whole system, which additionally hampers the analysis.

To overcome the latter problem, we recently developed a methodology for the analysis of calculated vibrational spectra in terms of rigorously defined localized vibrations.[50,51] By performing a unitary transformation of the normal modes contributing to one band, a set of localized modes is

obtained. Localized modes—in contrast to the delocalized normal modes—are in general dominated by a vibration on a single residue, and localized modes on different but homologous residues are found to be very similar. Therefore, these localized modes significantly simplify the interpretation of calculated vibrational spectra of large molecules and make it possible to analyze them in terms of vibrational frequencies and intensities of localized modes and the couplings between them.

In this paper, we analyze the calculated ROA spectra of polypeptides in terms of localized vibrations to understand the generation of the ROA signals in polypeptides and proteins. Our focus in this work is on helical elements of protein secondary structure. Although such helices, in particular α helices and 3_{10}-helices, are important secondary-structure elements in proteins in their native state, helical motifs are also very common in intermediate states during protein folding and in disordered polypeptides and proteins. Here, we select regular secondary-structure elements as a first target, and therefore consider model polypeptides in α-helical and 3_{10}-helical conformations. By comparing these conformations, it is possible to study two well-defined secondary-structure elements and to investigate how the ROA spectra are affected by switching between them.

This work is organized as follows. In the Results and Discussion, the theoretical background is briefly summarized, the construction of α-helical and 3_{10}-helical structural models is discussed, the general features of the calculated ROA spectra of the helical polypeptides are discussed, and the total intensities of the bands in these spectra and their band shapes are analyzed. Next, the calculated spectrum of the α helix is compared to the available experimental spectra of α-helical (all-*S*)-polyalanine, and then characteristic ROA signatures of 3_{10}-helices are discussed. Finally, a summary and concluding remarks are given in the Conclusion.

Results and Discussion

Theoretical background: For the ab initio calculation of vibrational spectra, one commonly employs the harmonic approximation.[37,52] Within this approximation, the normal modes $\boldsymbol{Q}_p$ are obtained as eigenvectors of the mass-weighted molecular Hessian matrix $\boldsymbol{H}^{(m)}$, which contains the second derivatives of the total electronic energy of the considered molecule with respect to Cartesian nuclear coordinates. The corresponding eigenvalues equal the squared angular frequencies of the vibrations, $\omega_p^2 = 4\pi^2\nu_p^2$, in which ν_p is the vibrational frequency corresponding to the normal mode $\boldsymbol{Q}_p$.

Within the semiclassical framework usually adopted to treat Raman and ROA spectroscopy,[19,53] and under the assumption that the molecular electronic ground state is nondegenerate and that the photon energy of the incident laser light is far away from any electronic excitation energy of the molecule, one obtains Equation (1) for the ROA backscattering intensity difference associated with the normal mode $\boldsymbol{Q}_p$:[19]

$$I_p = (I^{\mathrm{R}} - I^{\mathrm{L}})_p \propto \frac{32}{c}\left[3\beta(\boldsymbol{G}')_p^2 + \beta(\boldsymbol{A})_p^2\right] \tag{1}$$

in which c is the speed of light and the anisotropic ROA invariants $\beta(\boldsymbol{G}')^2$ and $\beta(\boldsymbol{A})^2$ are given by Equation (2):

$$\beta(\boldsymbol{G}')_p^2 = \frac{1}{2}\sum_{\alpha\beta}\left[3\left(\frac{\partial\alpha_{\alpha\beta}}{\partial\boldsymbol{Q}_p}\right)_0\left(\frac{\partial G'_{\alpha\beta}}{\partial\boldsymbol{Q}_p}\right)_0 - \left(\frac{\partial\alpha_{\alpha\alpha}}{\partial\boldsymbol{Q}_p}\right)_0\left(\frac{\partial G'_{\beta\beta}}{\partial\boldsymbol{Q}_p}\right)_0\right]$$
$$\beta(\boldsymbol{A}')_p^2 = \frac{1}{2}\omega_L\sum_{\alpha\beta\gamma\delta}\varepsilon_{\alpha\gamma\delta}\left(\frac{\partial\alpha_{\alpha\beta}}{\partial\boldsymbol{Q}_p}\right)_0\left(\frac{\partial A_{\alpha,\gamma\delta}}{\partial\boldsymbol{Q}_p}\right)_0 \tag{2}$$

in which $\boldsymbol{\alpha}$ is the electric-dipole–electric-dipole polarizability tensor, $\boldsymbol{G}'$ is the electric-dipole–magnetic-dipole polarizability tensor, $\boldsymbol{A}$ is the electric-dipole–electric-quadrupole polarizability tensor. Greek indices $\alpha,\beta,\gamma,\delta$ label Cartesian components (x,y,z), ω_{L} is the angular frequency of the incident laser beam, and $\varepsilon_{\alpha\gamma\delta}$ is an element of the antisymmetric Levi–Civita tensor. The subscript "0" indicates that the derivative is evaluated at the equilibrium structure $\boldsymbol{R}_0$ of the molecule. Note that, as is common in theoretical studies, in Equation (1) proportionality constants that depend on the precise experimental conditions have been neglected.

To analyze the vibrational spectra of polypeptides and proteins in terms of localized modes,[50,51] one considers a subset of k normal modes, which are usually those modes that contribute to one band in the vibrational spectrum. These normal modes are collected in the matrix $\boldsymbol{Q}^{\mathrm{sub}}$. By means of a unitary transformation $\boldsymbol{U}$ they can then be transformed to a set of localized modes $\tilde{\boldsymbol{Q}}^{\mathrm{sub}}$ [Eq. (3)],

$$\tilde{\boldsymbol{Q}}^{\mathrm{sub}} = \boldsymbol{Q}^{\mathrm{sub}}\boldsymbol{U} \tag{3}$$

in which the unitary transformation is chosen in such a way that it yields the "most localized" transformed modes. Here and in the following, the tilde is used to denote the localized modes, or other quantities that are defined with respect to these localized modes. The localization is achieved by maximizing $\xi(\tilde{\boldsymbol{Q}}^{\mathrm{sub}}) = \xi(\boldsymbol{Q}^{\mathrm{sub}}\boldsymbol{U})$, in which $\xi(\tilde{\boldsymbol{Q}}^{\mathrm{sub}})$ is a suitably defined criterion that measures how localized a set of transformed modes $\tilde{\boldsymbol{Q}}^{\mathrm{sub}}$ is.[50] Here, we applied the atomic-contribution criterion introduced in ref. [50].

Even though these localized modes are not eigenvectors of the mass-weighted Hessian $\boldsymbol{H}^{(m)}$, they are useful for the interpretation and analysis of calculated vibrational spectra.[51] For polypeptides and proteins, in which the normal modes are in general delocalized combinations of nuclear distortions on different amino acid residues, the localized modes will each be dominated by a vibration of one single residue. Furthermore, the localized modes on different residues will involve similar atomic displacements (i.e., the set of localized modes obtained for one vibrational band will consist of modes that are very similar, but are located on different residues).

Construction of secondary-structure elements: To investigate the ROA signatures of α-helical and 3_{10}-helical secondary-structure elements in proteins, we constructed model polypeptides that exhibit those specific structural features. Here, we chose alanine polypeptides, since alanine represents the smallest chiral amino acid, and since it is commonly believed that in the ROA spectra the signals that are due to the side chain average out due to conformational flexibility. To support an α helix and a 3_{10}-helix, rather large polypeptides containing twenty amino acid residues are required, since for smaller helices distorted helices are obtained.[41] Therefore, we employed a polypeptide consisting of twenty (*S*)-alanine residues, denoted Ala_{20}, as a model system. For this polypeptide, both an α-helical and a 3_{10}-helical structure have been considered.

The largest molecules for which accurate ab initio calculations of ROA spectra have been performed so far are two diastereomers of helical decaalanine.[41] Therefore, the polypeptides considered here represent the largest systems for which accurate ROA calculations have been performed to date.

All spectra have been calculated for isolated molecules and solvation effects have not been considered in our calculations, even though the ROA spectra of polypeptides are known to be sensitive to solvent effects.[28] However, as was discussed in ref. [51], continuum solvation models, which are the simplest and most efficient way of incorporating solvent effects in quantum chemical calculations, hardly affect the vibrational spectra of the Ala_{20} polypeptides considered here. Therefore, more sophisticated solvent models that explicitly include the molecular structure of the solvent will be required for an adequate description of the solvent effects on the ROA spectra of polypeptides (see, for example, ref. [54] for the description of solvent effects on vibrational spectra, and refs. [55–57] and references therein for other molecular properties). Although work in this direction is currently in progress in our laboratory, for our purposes here (i.e., for understanding of the generation of ROA bands in helical substructures) we may safely neglect solvent effects.

Calculation of ROA spectra for helical polypeptides: The calculated ROA spectra for both the α-helical and the 3_{10}-helical Ala_{20} in the region between 1100 and 1800 cm^{-1}, which comprises the bands that are commonly used to investigate polypeptides and proteins, are shown in Figure 1a. For the analysis of these spectra in terms of localized modes, it is first necessary to assign the individual normal modes to characteristic bands. This assignment can be performed by considering the wavenumbers of the transitions, which in most cases are clearly separated for the different bands, and by collecting modes for which the contributions of certain groups of atoms show a similar pattern. Here, we apply the same assignment as in our previous study.[51] The eight considered bands, the corresponding wavenumber ranges, and the maxima and minima of these bands are listed in Table 1.

Since ROA spectra contain both positive and negative peaks, one band does not always correspond to a single peak as is the case for the IR and Raman spectra;[51] more complicated band shapes such as couplets can arise. This also makes it more difficult to identify the individual bands in the plotted spectra. Therefore, Figure 1b shows the calculated ROA spectra, in which the assignment of modes to characteristic bands is indicated by boxes. The band shapes found for each of the bands are included in Table 1. Before analyzing how these band shapes arise, we will first consider the total band intensities (i.e., the sum of the intensities of all modes in one band). Positive and negative peaks can cancel each other out, so that the band shapes found in the calculated spectra sensitively depend not only on the positions of the individual vibrational transitions but also on the line broadening that is applied to visualize the spectra. Therefore, these total band intensities can be expected to be less sensitive to inaccuracies in the computational methodology. Since it was not clear whether these errors, in particular the use of the harmonic approximation, are homogeneous for close-lying peaks, it was suggested earlier to interpret calculated ROA spectra of large molecules in terms of the total intensities of characteristic bands.[41] To visualize these total band intensities, Figure 1c shows the calculated ROA spectra of Ala_{20} using rectangular peaks that indicate the total intensities of the bands. In the following, we analyze how these total band intensities and the individual band shapes arise. For this analysis, we focus on the bands that are most sensitive to secondary structure (i.e., the amide I and amide II bands as well as the bands in the extended amide III region). For the sake of completeness, we provide the analysis of the total band intensities and of the band shapes for the symmetric and antisymmetric CH_3 bending bands and for the skeletal C^{α}–N stretching band in the Supporting Information.

Analysis of total band intensities: First, we analyze the total intensities of the characteristic ROA bands. Whereas the intensities of the individual normal modes contributing to one of these bands differ significantly and can show rather complicated patterns that are reflected in the observed band shapes, the corresponding localized modes are much simpler to interpret. Since the localized modes are in general similar vibrations on different residues, they also have very similar ROA intensities, with deviations only occurring at the terminal residues. Therefore, to analyze the total band intensities, it is generally sufficient to investigate only one representative localized mode on one of the central residues. Differences in the total band intensities between the two conformers are then largely reflected in differences in the ROA intensity of these representative localized modes. The ROA intensities of all considered normal modes as well as those of the corresponding localized modes are listed in the Supporting Information.

In the following, we employ one of the localized modes with the main contribution on residue 9 or 10 for the analysis of the total band intensities. First, to understand the atomic displacements that are important for the bands in the ROA spectra, these can be visualized for these represen-

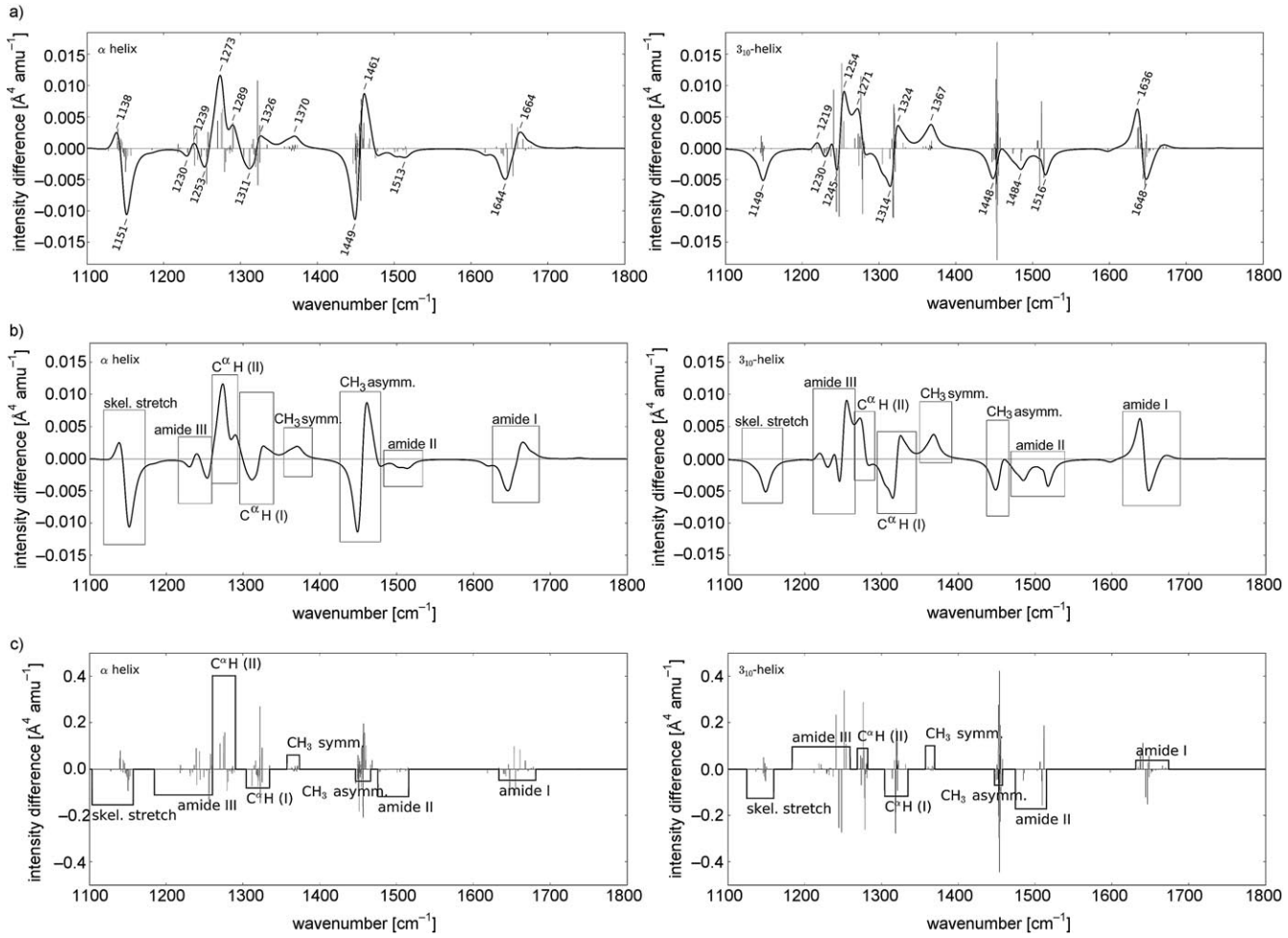

Figure 1. a) Calculated backscattering ROA spectra of α-helical (left) and 3_{10}-helical (right) Ala_{20}. The spectra have been plotted using a Lorentzian line width of 15 cm^{-1}. Individual peaks have been included as a line spectrum scaled by 0.04. b) Assignment of the individual modes to characteristic bands. c) Band-averaged ROA spectra. The heights of the rectangular peaks indicate the total intensities of the bands.

tative localized modes. Since only a small number of atoms contribute to the localized modes, it is sufficient to show only a small part of the polypeptides, which simplifies the visualization considerably.[50]

Second, the ROA intensities of the localized modes are decomposed into local contributions of groups of atoms using the scheme proposed by Hug[44] to understand which atomic displacements and which groups of atoms are responsible for the ROA signals. In this scheme, the ROA intensity $\tilde{I}_p$ of the p-th mode is decomposed as [Eq. (4)]:

$$\tilde{I}_p = \sum_{AB} [\tilde{I}_p]_{AB} \qquad (4)$$

with the indices A and B running over suitably chosen groups of atoms (see below for examples). Since different groups of atoms are important for each of the characteristic bands, the groups of atoms that are used for this decomposition are chosen differently for different bands in the following so as to capture the important contributions while keeping the number of groups as small as possible. Whereas the diagonal terms $[\tilde{I}_p]_{AA}$ represent contributions that are solely due to the atoms in the group A, the off-diagonal terms $[\tilde{I}_p]_{AB}$ arise from the coupling between atoms in groups A and B. These local contributions can be visualized as *group coupling matrices* by representing the local contributions as circles with an area proportional to the size of the local contributions (filled circles are used for positive terms, whereas empty circles are used for negative ones; see Figures 2–4).

Amide I band: The amide I band appears for the considered molecules approximately in the region between 1630 and 1670 cm^{-1}. The representative localized modes, which are shown in Figure 2b, mainly involve a stretching vibration of C=O group of residue 9, with contributions of a bending vibration of the adjacent N–H group of residue 10. As the figure shows, these atomic displacements are almost identical for the localized modes of α-helical and 3_{10}-helical Ala_{20}.

For the α helix, the total amide I band intensity is weakly negative, whereas for the 3_{10}-helix a weakly positive total band intensity is found (see Table 1 and Figure 1). This sign change is reflected in the ROA intensities of the considered

Table 1. Wavenumber ranges, band maxima or minima, total ROA intensity, and ROA band shapes for the characteristic bands in the ROA spectra of α-helical and 3_{10}-helical Ala_{20}. For the band shapes, "couplet +/−" indicates a couplet that is positive at low wavenumbers and negative at high wavenumbers, whereas "couplet −/+" indicates a couplet that is negative at low wavenumbers and positive at high wavenumbers.

	Range [cm^{-1}]	Max/min [cm^{-1}]	Total ROA intensity [10^{-3} $Å^4 amu^{-1}$]	Band shape
α helix				
amide I	1633–1681	1644, 1664	−48.1	couplet −/+
amide II	1468–1515	1513	−118.6	negative peak
$C^{\beta}H_3$ asymm. bend	1446–1466	1449, 1461	−52.2	couplet −/+
$C^{\beta}H_3$ symm. bend	1356–1373	1370	61.2	positive peak
C^{α}–H bending (I)	1304–1334	1311, 1326	−81.5	couplet −/+
C^{α}–H bending (II)	1257–1290	1273, 1289	402.8	two positive peaks
amide III	1184–1260	1253	−110.9	two negative peaks
skeletal C^{α}–N stretch	1103–1156	1138, 1151	−153.6	couplet +/−
3_{10}-helix				
amide I	1631–1674	1636, 1648	38.6	couplet +/−
amide II	1474–1515	1484, 1516	−171.4	two negative peaks
$C^{\beta}H_3$ asymm. bend	1447–1457	1448	−69.2	negative peak
$C^{\beta}H_3$ symm. bend	1357–1369	1367	100.9	positive peak
C^{α}–H bending (I)	1304–1334	1314, 1324	−116.6	couplet −/+
C^{α}–H bending (II)	1268–1282	1271	90.0	positive peak
amide III	1183–1259	1254	96.4	couplet −/+
skeletal C^{α}–N stretch	1124–1159	1149	−125.5	negative peak

localized modes, which are -5.93 $Å^4 amu^{-1}$ for the α helix and $+1.47$ $Å^4 amu^{-1}$ for the 3_{10}-helix. The decompositions of these ROA intensities are shown in Figure 2b as group coupling matrices. The largest contributions are the positive diagonal term associated with the C=O group of residue 9 (i.e., the group which also shows largest atomic displacements in the considered localized modes) as well as the negative off-diagonal terms associated with the coupling between this C=O group on residue 9 and the N−H groups on residues 10 and 11. The differences between the α helix and the 3_{10}-helix can be mainly attributed to the increase of the positive diagonal contribution of the C=O group of residue 9. Note that, as this C=O group is not chiral, this increase must be due to changes of the derivative of the required polarizability tensors with respect to the C=O stretching vibration (i.e., it is due to changes in the electronic structure of the chiral molecule, which are probed by the C=O stretching vibration).[33]

Amide II band: The amide II band is found between approximately 1470 and 1520 cm^{-1}. As for the amide I band, we have considered the localized mode, which has its main contribution on the amide group connecting residues 9 and 10. The localized amide II modes, which are shown in Figure 2c, are an out-of-phase combination of an N−H bending vibration and of an amide C−N stretching vibration. As for the amide I modes, the localized modes obtained for the two considered conformers are almost identical.

For both the α-helical and the 3_{10}-helical Ala_{20}, the total intensities of the amide II band are negative and of medium magnitude. However, in the spectra shown in Figure 1, the amide II mode appears only weakly negative for the α helix. On the one hand, this is the case because the amide II band is rather broad; on the other hand, it is because the normal modes at low wavenumbers are close to the asymmetric CH_3 bending modes, so that the low-wavenumber part of the amide II band is canceled by close-lying modes of the asymmetric CH_3 bending band. Even though the total band intensities are of the same order of magnitude, the ROA intensities of the localized modes differ significantly (see the Supporting Information). For the α helix, the localized modes on the central residues only show a small negative ROA intensity (around 2 $Å^4 amu^{-1}$), whereas the localized modes on the terminal residues show strongly negative ROA intensities. These localized modes at the terminal residues appear at wavenumbers below 1495 cm^{-1} and mainly contribute to those localized modes that appear in the low-wavenumber part of the amide II band. For the 3_{10}-helix, the localized modes show a more regular intensity distribution, so that the localized modes on central residues show stronger negative ROA intensities (around 10 $Å^4 amu^{-1}$), whereas the intensities of those on the terminal residues have a somewhat weaker negative ROA intensity. Therefore, the representative localized mode considered for the α helix has a weakly negative ROA intensity of -1.90 $Å^4 amu^{-1}$, whereas the one considered for the 3_{10}-helix has a stronger negative ROA intensity of -9.93 $Å^4 amu^{-1}$.

The group coupling matrices showing the decomposition of the ROA intensities of the considered amide II localized modes are given in Figure 2c. The largest contributions to the ROA intensities are those of the amide group connecting residues 9 and 10 (i.e., the diagonal terms associated with the C=O group of residue 9 and with the N−H group of residue 10 as well as the off-diagonal term describing the coupling between these two groups). This amide group, which is also where the considered localized modes have the largest atomic displacements, gives rise to a negative contribution to the ROA intensity. The off-diagonal terms describing the coupling of the C=O and N−H groups of residues 9 and 10, respectively, with the C=O group on residue 8 lead to positive contributions. The difference between the ROA intensities of the localized amide II modes of the two conformers is mainly due to the increased negative intensity of diagonal terms associated with the amide group connecting residues 9 and 10. Again, because this group and its vibration are achiral and because the localized modes are almost identical in the two conformers, the change in the ROA intensity must be caused by changes in the local electronic structure.

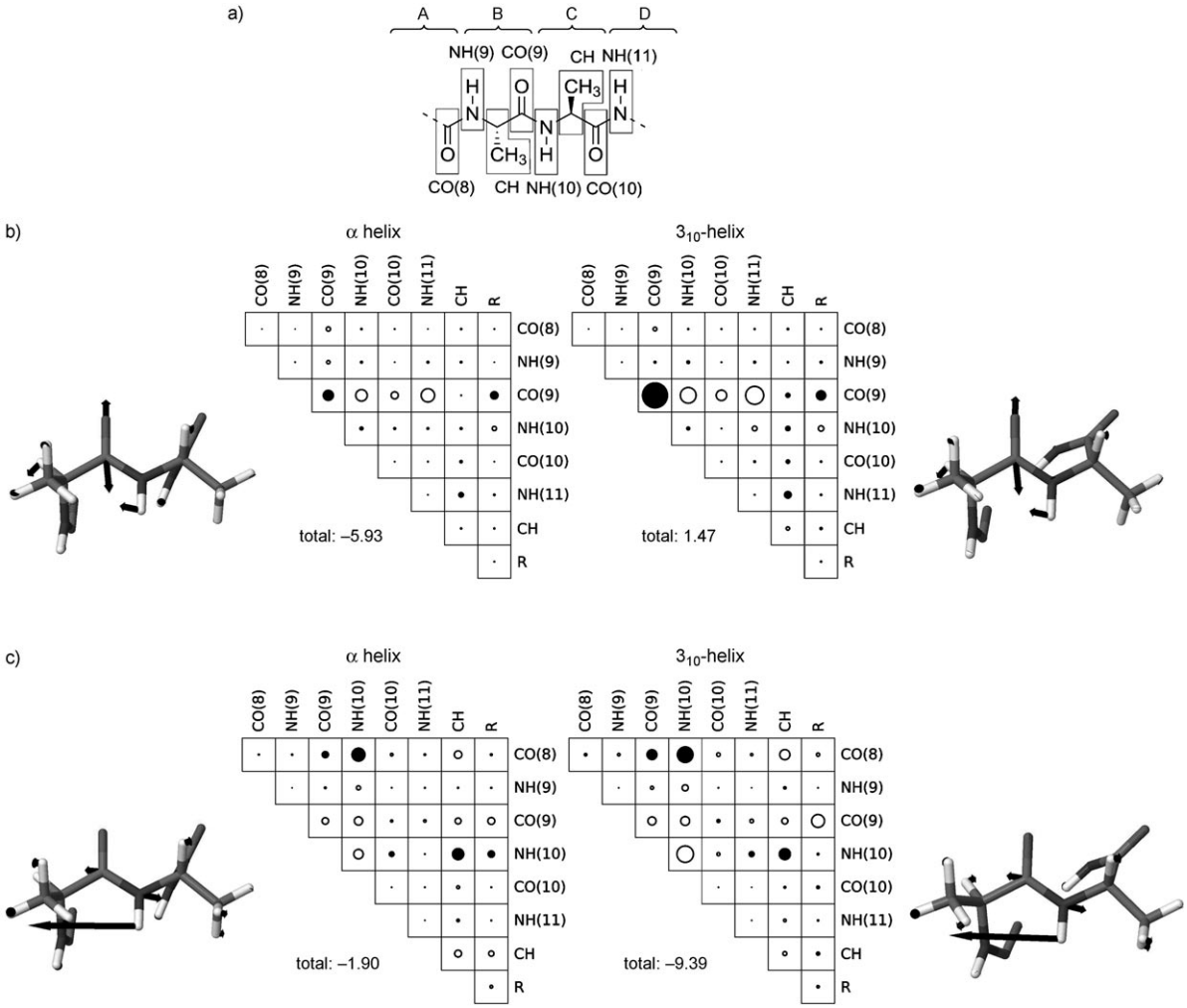

Figure 2. Analysis of the ROA intensities of representative amide I and amide II localized modes. a) Groups of atoms that are used for the decomposition into local contributions. All atoms not shown are collected in the group "R" (A = residue 8, B = residue 9, C = residue 10, D = residue 11). Considered b) amide I and c) amide II localized modes and group coupling matrices showing the decomposition of the ROA intensity of these modes into local contributions. The total ROA intensities of the localized modes [$Å^4 amu^{-1}$] are also given.

Bands in the extended amide III region: The bands appearing in the region between approximately 1200 and 1350 cm^{-1} are usually jointly referred to as the "extended amide III" region. For the polypeptides investigated here, three bands appear in this region that are all due to the mixing of the classical amide III vibration, which is an in-phase combination of the N–H bending and the C–N stretching vibrations of the amide group, and of the C^{α}–H bending modes. The representative localized modes obtained for each of these bands, which are denoted as C^{α}–H bending (I), C^{α}–H bending (II), and amide III, are shown in Figure 3b–d.

The localized modes shown for the C^{α}–H bending (I) band are mainly due to a bending vibration of the C^{α}–H group of residue 10, where the direction of the bending vibration is along the N–C^{α} bond, whereas those shown for the C^{α}–H bending (II) band are dominated by a C^{α}–H bending vibration that is perpendicular to the N–C^{α} bond. For both the C^{α}–H bending (I) and for the C^{α}–H bending (II) localized modes, there are additional contributions of the classical amide III vibrations of the adjacent amide groups (i.e., of the amide group connecting residues 9 and 10 and of the one connecting residues 10 and 11, as well as smaller contributions of asymmetric CH_3 bending vibrations). The representative localized modes shown for the amide III band are dominated by the classical amide III vibration of the amide group connecting residues 9 and 10. However, this classical amide III vibration strongly couples with C^{α}–H bending vibrations of residues 9 and 10 that are approximately perpendicular to the N–C^{α} bond. Furthermore, there are smaller contributions of asymmetric CH_3 bending vibrations of the side chains.

For the C^{α}–H bending (I) band, the localized modes obtained for the α helix and for the 3_{10}-helix are similar vibrations. However, for the C^{α}–H bending (II) and for amide III band, the localized modes differ for the two conformers. In particular, the degree of mixing between the classical amide III and the C–H bending vibrations changes if the secon-

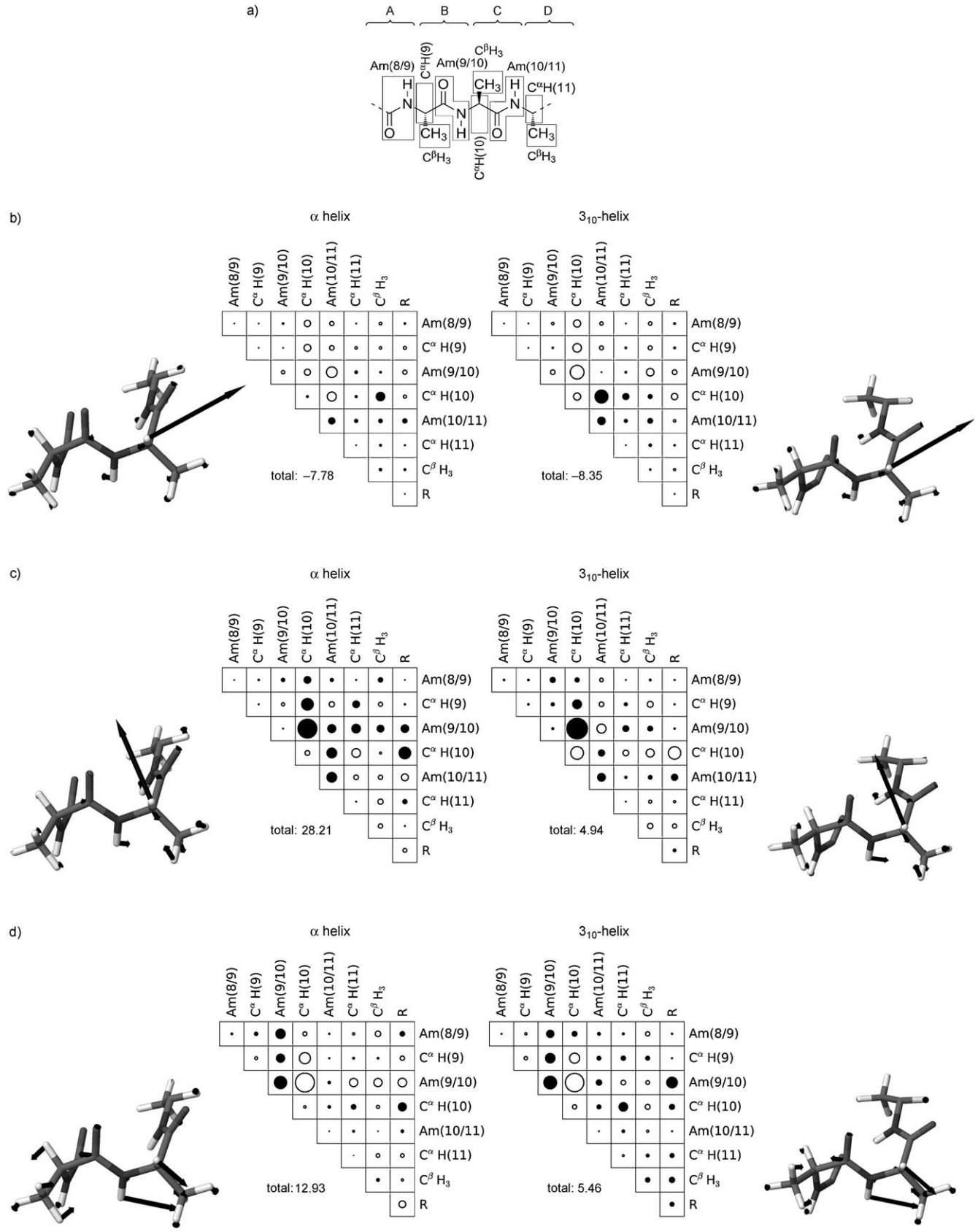

Figure 3. Analysis of the ROA intensities of representative localized modes for the bands in the extended amide III region. a) Groups of atoms that are used for the decomposition into local contributions. All atoms not shown are collected in the group "R" (A = residue 8, B = residue 9, C = residue 10, D = residue 11). Considered b) C–H bending (I), c) C–H bending (II), and d) amide III localized modes and group coupling matrices showing the decomposition of the ROA intensity of these modes into local contributions. The total ROA intensities of the localized modes [Å^{4}amu^{-1}] are also given.

dary structure changes. A more detailed discussion of the modes in the extended amide III region, and an analysis of this coupling between the C^{α}–H bending and the classical amide III vibrations by means of region-localized modes, which are obtained for the whole extended amide III region, were already given in ref. [51].

For the C^{α}–H bending (I) band, a negative total intensity is found for both the α helix and the 3_{10}-helix. The total intensities found for the two conformers are rather similar and of medium size. In accordance with this, the ROA intensities of the considered localized modes are also in both cases negative and of medium size (approximately -8 Å^{4}amu^{-1}). The decomposition of these localized-mode intensities is shown in Figure 3b. All of the diagonal contributions are rather small, and the largest contributions are due to the off-diagonal terms associated with the coupling of the C^{α}–H group of residue 10 with the adjacent amide groups and with the off-diagonal term associated with the coupling between these two amide groups. Even though both the total ROA intensity and the composition of the considered localized modes are quite similar for the two conformers, the magnitude of the local contributions differs. On the one hand, these differences can be caused by changes in the local electronic structure that lead to changes in the polarizability derivatives, but in contrast to the diagonal contributions, which are the most important for the amide I, amide II, and CH_3 bending bands considered above, the off-diagonal contributions are, on the other hand, also directly affected by the structural changes. The changes in the backbone dihedral angles result in a different orientation of the C^{α}–H group and the amide groups with respect to each other, and even if the polarizability derivatives along the displacements are unchanged for the individual groups, these changes in the relative orientation affect the resulting contributions to the ROA intensities.[19]

For the C^{α}–H bending (II) band, the total intensities differ significantly for the α helix and the 3_{10}-helix. Whereas a very strongly positive total intensity is found for the α helix, the 3_{10}-helix shows only a positive total intensity of medium size. This decrease in the total band intensity is also reflected in the ROA intensities of the localized modes considered. As the group coupling matrices in Figure 3c show, the main contributions to these ROA intensities originate from the off-diagonal coupling terms. For both helices, a large positive contribution is found for the term associated with the coupling of the C^{α}–H group of residue 10 with the amide group connecting residues 9 and 10. For the 3_{10}-helix, this positive contribution is partly canceled by negative contributions that are due to the diagonal term associated with the C^{α}–H group of residue 10 and the off-diagonal terms describing its couplings with other groups, including the parts of the helix that are not shown in the figure. This results in a significantly smaller positive ROA intensity in the 3_{10}-helix. For the C^{α}–H bending (II) band, the considered localized modes of the two helices differ, and in particular the degree of mixing between the C^{α}–H bending and the classical amide III vibration changes. This can be expected to significantly affect the corresponding local contributions and thus the total ROA intensities (i.e., the differences between the two structures are mainly caused by changes in the composition of the localized modes).

For the amide III band, a medium-sized negative total intensity is found for the α helix, whereas a total intensity of similar magnitude, but of positive sign, characterizes the 3_{10}-helix. This sign change is also found for the representative localized modes considered. However, the magnitude of the negative intensity found for the localized amide III mode of the α helix is larger than the magnitude of the positive ROA intensity of the localized mode obtained for the 3_{10}-helix. This is due to the fact that some of the localized modes at the C terminus for both helices have a large positive ROA intensity (see the Supporting Information). The group coupling matrices in Figure 3d show that in both cases, the largest contribution is, as for the C^{α}–H bending (II) band, the off-diagonal term associated with the coupling of the amide group connecting residues 9 and 10 with the C^{α}–H group of residue 10. However, in contrast to the C^{α}–H bending (II) band, this term now has a negative sign. In addition, there are contributions of the diagonal term of the amide group as well as of the off-diagonal term describing its coupling with the C^{α}–H groups. For the 3_{10}-helix, the off-diagonal terms for the coupling of the amide group connecting residues 9 and 10 with other groups, including those not shown in the figure, give more positive contributions, which cancel the dominant negative contribution.

For all three bands in the extended amide III region, the total intensities arise through a different mechanism than that described for the other bands so far. Whereas for the amide I, amide II (see above), and CH_3 bending bands (see Supporting Information) the ROA intensities of the representative localized modes are each due to the diagonal contribution of one single group of atoms—an amide group for the amide I and II bands and the side-chain methyl group for the C^{α}–H bending bands—off-diagonal terms that arise from the coupling of two different groups of atoms are the most important for the extended amide III region. In particular, the coupling of the classical amide III vibration and of a C^{α}–H bending vibration is decisive for the total band intensities. This also explains the large sensitivity of the modes in the extended amide III region, in particular of the C^{α}–H bending (II) and of the amide III band, to structural changes. On the one hand, the size of the coupling terms depends on the composition of the localized modes, and on the other hand, the size of the off-diagonal terms is directly related to the orientation of the vibrating groups with respect to each other. These changes in the coupling between C^{α}–H bending vibrations and the classical amide III mode that are induced by changes in the secondary structure result in a redistribution of the ROA intensity between the bands in the amide III region. Note that while the total intensities of the C^{α}–H bending (II) and of the amide III band differ significantly for the α helix and the 3_{10}-helix, the sum of the total band intensities is rather similar for both conformers.

Analysis of the band shapes: To analyze the band shapes, it is necessary to consider how the localized modes couple to normal modes, and how the ROA intensity is distributed among these normal modes. The coupling of the localized modes to normal modes is determined by the vibrational coupling matrix $\tilde{\boldsymbol{\Omega}}$, which is related to the Hessian matrix in the basis of the localized modes.[50] For the polypeptides considered here, this vibrational coupling matrix has for all considered bands a rather simple structure. Its elements (i.e., the vibrational coupling constants) only depend on the distance between the residues on which the localized modes are located.[50,51] Deviations only occur for the terminal residues. Furthermore, the coupling constants between localized modes on residues that are separated by more than three residues are usually negligible. Therefore, it is sufficient to consider only the couplings between one representative localized mode with those localized modes on neighboring residues. Table 2 lists the coupling constants between the localized mode on residue 8 and those on residues 9, 10, 11, and 12.

Table 2. Coupling constants for the interaction of the localized modes on residue 8 with those on residues 9, 10, 11, and 12. All values are in cm^{-1}. The phase of the localized modes is chosen such that localized modes on neighboring residues have the same phase.

	8↔9	8↔10	8↔11	8↔12
α helix				
amide I	+7.9	−2.3	−4.2	−0.4
amide II	−2.8	−3.5	−0.6	+0.8
$C^{\beta}H_3$ symm. bend	−0.2	+0.1	−0.2	0.0
$C^{\alpha}H$ bend (I)	−1.1	+0.3	+0.1	−0.3
$C^{\alpha}H$ bend (II)	+2.7	−0.8	+1.3	−0.1
amide III	−7.5	+1.0	+0.6	+0.8
3_{10}-helix				
amide I	+2.7	−3.7	−0.8	−0.6
amide II	−6.2	−3.5	+1.1	−0.3
$C^{\beta}H_3$ symm. bend	−0.3	+0.1	−0.2	0.0
$C^{\alpha}H$ bend (I)	+0.1	+0.5	−0.4	0.0
$C^{\alpha}H$ bend (II)	+1.8	−1.2	+0.2	−0.1
amide III	−7.2	+2.3	+0.3	−0.1

By diagonalizing the vibrational coupling matrix $\tilde{\boldsymbol{\Omega}}$, one obtains the vibrational frequencies of the normal modes as eigenvalues and the coefficients U_{pr} of the normal modes in the basis of the localized modes as eigenvectors.[50,51] The p-th normal mode $\boldsymbol{Q}_p$ is then obtained as $\boldsymbol{Q}_p = \Sigma_r U_{pr} \tilde{\boldsymbol{Q}}_r$, in which $\tilde{\boldsymbol{Q}}_r$ denotes the r-th localized mode (i.e., the coefficient U_{pr} gives the contribution of the r-th localized mode to the p-th normal mode).

Depending on the structure of the coupling matrix, different coupling patterns will arise. In the simplest case, the nearest-neighbor coupling constant is large, whereas the other coupling constants are negligible. For degenerate localized modes, this leads to a (nodeless) normal mode, which is an in-phase combination of localized modes, at one end of the band, and a normal mode with a maximum number of nodes, which is an out-of-phase combination of localized modes with alternating phases, on the other end of the band. Between these two extremes combinations of localized modes with a steadily increasing number of nodes appear. For a positive sign of the nearest-neighbor coupling constant, the nodeless in-phase combination appears at higher wavenumbers and the out-of-phase combination appears at lower wavenumbers, while for a negative sign the opposite order is obtained. The separation between the resulting normal modes depends on the magnitude of the coupling constant. In general, the second- and third-nearest-neighbor coupling constants will not be negligible, which will modify the coupling pattern described above. Furthermore, if the nearest-neighbor coupling constant is not the largest, a different coupling pattern will be found. Nevertheless, in most cases the simple coupling pattern described here provides a useful starting point for the discussion of the coupled normal modes.

Once it is known how the localized modes couple to normal modes, the ROA intensity of the p-th normal mode can be obtained as [Eq. (5)]:[51]

$$I_p = \sum_{qr} U_{pq} U_{pr} [\tilde{I}]_{qr} \tag{5}$$

in which U_{pq} and U_{pr} are the coefficients giving the contributions of the q-th and r-th localized mode to the considered normal mode, respectively, and $[\tilde{I}]_{qr}$ is an element of the *intensity coupling matrix* corresponding to these localized modes. The elements of the intensity coupling matrix depend on products of polarizability tensor derivatives with respect to the localized modes (see the Supporting Information for details).[51] For each of the considered bands, graphical representations of the sub-block of the intensity coupling matrices corresponding to the localized modes on residues 7 to 12 are shown in Figure 4. Note that in these plots the elements $[\tilde{I}]_{qr}$ and $[\tilde{I}]_{rq}$ have been added, so that only an upper triangular matrix is retained. As for the vibrational coupling matrix, the intensity coupling matrices have a rather simple structure for the regular polypeptides considered here. The elements corresponding to the same distance between the localized modes (i.e., those on the secondary diagonals) are very similar. However, in contrast to the vibrational coupling constants, the elements of the intensity coupling matrices depend only on the orientation of the localized modes with respect to each other, but not on their distance, and therefore they do not decrease with increasing separation between the localized modes.

For a given normal mode, the ROA intensity is then obtained as a sum of elements of the intensity coupling matrix, each multiplied by a coefficient $U_{pq}U_{pr}$ depending on the composition of the normal mode in terms of localized modes. For each pair of localized modes, this coefficient is given by the product of the contributions of these two localized modes to the considered normal mode. If these two localized modes appear with the same phase, this product will be positive, whereas it will be negative if they have opposite phase. Therefore, for the nodeless in-phase combination of

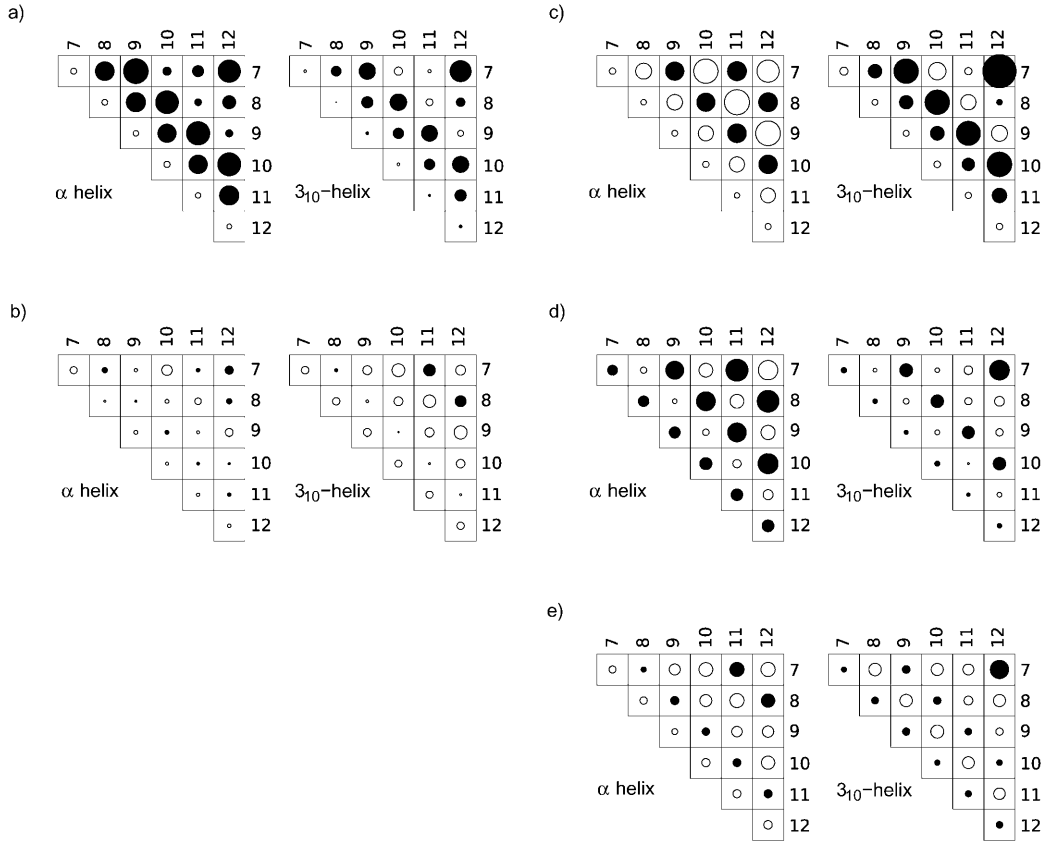

Figure 4. Sub-block of the intensity coupling matrices corresponding to the localized modes on residues 7 to 12 for all considered bands in the ROA spectra of α-helical and 3_{10}-helical Ala_{20}. The phase of the localized modes is chosen such that localized modes on neighboring residues have the same phase. a) Amide II, b) amide II, c) C–H bending (I), d) C–H bending (II), and e) amide III.

the localized modes, all intensity coupling matrix elements appear with a positive sign. On the other hand, for the out-of-phase combination with a maximum number of nodes, this product will be negative for localized modes on neighboring residues and those separated by an even number of residues, and it will be positive for those separated by an odd number of residues. Therefore, the intensity coupling matrix elements on the first, third, fifth, and so on secondary diagonal will enter with a negative sign, whereas those on the second, fourth, and so on secondary diagonal will appear with a positive sign. In general, for normal modes that have only few nodes with respect to the localized modes, most intensity coupling matrix elements will enter with a positive sign, whereas a larger number of them enter with a negative sign if the number of nodes increases.

Now the band shapes will be analyzed by first investigating which combinations of localized modes arise due to the vibrational coupling constants, and by then analyzing how the ROA intensity is distributed among these modes due to the intensity coupling terms. To illustrate the normal modes that arise due to the vibrational coupling, the Supporting Information contains plots that for each of the considered bands schematically show the coupled modes obtained from diagonalizing the sub-block of the vibrational coupling matrix that corresponds to residues 7 to 12. Even though the coupling patterns are in general more complicated than in the simple case discussed above, in which only the nearest-neighbor coupling is considered, it turns out that this simplest case is usually sufficient for a qualitative understanding. For analyzing the distribution of the ROA intensity among the normal modes, we also only consider the sub-block of the intensity coupling matrix corresponding to the central residues 7 to 12. Note that even though the intensity coupling matrix elements corresponding to larger distances between the localized modes do not decrease in size, they nevertheless become less important for the intensities of the coupled modes and thus for the band shapes since the number of such intensity coupling matrix elements decreases. Furthermore, these matrix elements usually give contributions of the opposite sign for close-lying normal modes and thus average out so that they do not significantly affect the overall band shapes.

Amide I band: For the α-helical Ala_{20}, a couplet, which is negative at low wavenumbers and positive at higher wavenumbers, is found for the amide I band. In contrast, the opposite band shape (i.e., a couplet that is positive at low wavenumbers and negative at high wavenumbers) is found for the 3_{10}-helical Ala_{20}. This different band shape can be understood by considering the vibrational coupling con-

stants in Table 2 as well as the intensity coupling matrices shown in Figure 4a.

For the α helix, the vibrational coupling is mainly determined by the nearest-neighbor coupling constant, which is significantly larger than the couplings between localized modes on residues that are further apart. Therefore, one obtains the simple coupling pattern that was described above. Since the nearest-neighbor coupling constant is positive, the in-phase combination of the localized modes and combinations with only few nodes appear at higher wavenumbers, whereas the out-of-phase combination and those with a larger number of nodes appear at lower wavenumbers. As the intensity coupling matrix is dominated by positive terms, the normal modes at higher wavenumbers, which have fewer nodes and for which most of the products $U_{pq}U_{pr}$ in Equation (5) are positive, have a positive ROA intensity, whereas those at lower wavenumbers, which have more nodes and for which a large number of the products $U_{pq}U_{pr}$ are negative, show a negative ROA intensity.

For the 3_{10}-helix, the intensity coupling matrix elements are somewhat smaller in magnitude, but for the α helix, the intensity coupling matrix is dominated by positive elements. However, the structure of the vibrational coupling matrix is different. Whereas for the α helix the nearest-neighbor coupling constant is larger than the other coupling constants, for the 3_{10}-helix the second-nearest-neighbor coupling, which corresponds to one complete turn of the helix, is the largest in magnitude.[51] This, and the fact that this second-nearest-neighbor coupling constant has a negative sign, leads to a different coupling pattern. The normal modes with few nodes, which have a positive ROA intensity, now appear at lower wavenumbers, whereas those with many nodes and thus a negative ROA intensity are found at higher wavenumbers. Therefore, the different structure of the vibrational coupling matrix leads to a couplet which is opposite to the one found for the α helix.

Note that for both the α helix and the 3_{10}-helix the off-diagonal elements of the intensity coupling matrix are very large compared to the ROA intensities of the localized modes (i.e., the diagonal elements of the intensity coupling matrix). This leads to large (positive and negative) ROA intensities of the individual normal modes, whereas those of the localized modes are comparably small—as are the total amide I band intensities discussed previously. Furthermore, the vibrational coupling constants are rather large, which leads to a large splitting between the normal modes with positive and negative ROA intensities so that their ROA intensities do not cancel out and a strong couplet is observed in the calculated ROA spectra.

Amide II band: For the α helix, the amide II band is a rather broad peak with only a weak intensity, and it is therefore hardly visible in our calculated ROA spectrum. This is due to the rather large first- and second-nearest-neighbor vibrational coupling constants of -2.8 and $-3.5\,cm^{-1}$, respectively, which lead to a significant splitting between the normal modes, so that these are spread out over a large wavenumber range. As discussed above, the amide II normal modes at lower wavenumbers are close to the asymmetric CH_3 bending band, so that the intensity of these modes is canceled out. Moreover, the off-diagonal elements of the amide II intensity coupling matrix (see Figure 4b) are small, so that the coupling terms only slightly affect the distribution of ROA intensity among the normal modes and similar intensities are obtained for the normal modes and for the localized modes.

For the 3_{10}-helix, the amide II band is split into two negative peaks with minima at 1484 and $1516\,cm^{-1}$. The vibrational coupling is in this case mainly determined by the large nearest-neighbor coupling constant of $-6.2\,cm^{-1}$, which leads to a coupling pattern as described earlier, in which the nodeless in-phase combination appears at lower wavenumbers, whereas the out-of-phase combination is found at higher wavenumbers. However, the intensity coupling matrix now has a different structure than in the case of the amide I band. The elements of the intensity coupling matrix corresponding to nearest-neighbor residues are negligible, whereas those for second- and third-nearest-neighbor residues are negative. This leads to the observed splitting. Both for the nodeless in-phase combination and for the out-of-phase combination with alternating phases (in which localized modes on second-nearest-neighbor residues have the same phase) these second-nearest-neighbor intensity coupling terms enter with a positive coefficient. Therefore, the negative ROA intensity of these normal modes at the low and at the high wavenumber ends of the amide II band is amplified. It should be noted that compared to the amide I band the magnitude of the intensity matrix elements is small, so that the negative intensity is only redistributed within the band, whereas a strong couplet arises for the amide I band.

Bands in the extended amide III region: The extended amide III region is known to be very sensitive to secondary structure,[27,28,58,59] and consequently not only the total band intensities in the calculated ROA spectra of α-helical and 3_{10}-helical Ala_{20} show significant differences, but also the band shapes. These will be discussed separately for each of the three characteristic bands in this region.

In the case of the C^{α}–H bending (I) band, for both helices a couplet, negative at low wavenumbers and positive at high wavenumbers, is found. Since in both cases the total band intensity is weakly negative, the negative part of this couplet is somewhat more pronounced. However, even though the band shapes are similar, these couplets are generated in different ways. For the α helix, the nearest-neighbor vibrational coupling constant of $-1.1\,cm^{-1}$ is small, but significantly larger than the other couplings, so that the vibrational coupling follows the simple coupling pattern discussed above. As the dominant coupling constant is negative, the in-phase combination occurs at lower wavenumbers and the out-of-phase combination at higher wavenumbers. The intensity coupling matrix shown in Figure 4c has an alternating structure with negative elements for the first-, third-, and fifth-

nearest-neighbor couplings and positive ones for the second- and fourth-nearest-neighbor couplings. For the out-of-phase combination at higher wavenumbers, the negative elements are multiplied by a negative coefficient and the positive elements by a positive coefficient so that a large positive intensity is obtained. For the in-phase combination, the negative nearest-neighbor and third-nearest-neighbor contributions dominate over the remaining positive ones. Altogether, this results in the observed couplet.

For the 3_{10}-helix, the vibrational coupling constants are different, and the second-nearest-neighbor coupling constant is the largest and has a positive sign. As for the amide I band, this results in the opposite order for the coupled normal modes. However, also the intensity coupling matrix is different. The nearest-neighbor intensity coupling matrix elements change their sign and are positive for the 3_{10}-helix, and the magnitude of the positive second-nearest-neighbor terms increases, whereas the magnitude of the negative third-nearest-neighbor terms decreases. This results in an inversion of the intensity coupling contributions of the in-phase and out-of-phase combinations, so that in the end the same couplet as for the α helix is obtained.

The C^{α}–H bending (II) band has for the α helix a strongly positive total intensity and is split into two peaks, a larger one with its maximum at 1273 and a smaller one at 1289 cm^{-1}. Again, the vibrational coupling is determined by the nearest neighbor coupling of $+2.7\ cm^{-1}$, thus leading to the coupling pattern discussed earlier. The intensity coupling matrix given in Figure 4d has very small elements for the nearest-neighbor coupling, whereas those for the second-nearest-neighbor coupling are large and positive. As discussed for the amide II band in the 3_{10}-helix, this results in an increased intensity for both the in-phase and the out-of-phase combinations at high and at low wavenumbers, respectively, and thus explains the two maxima found for the α helix. For the 3_{10}-helix, only a single positive peak is obtained. Compared to the α helix, both the vibrational coupling constants and the intensity coupling terms are significantly smaller. Therefore, the normal modes are very close and the intensity coupling terms largely cancel out.

For the amide III band, a negative total intensity is obtained for the α helix, and a positive one for the 3_{10}-helix. For the former, the amide III band is split into two negative peaks with minima at 1230 and 1253 cm^{-1}, whereas for the latter, a couplet with a weak negative peak at 1245 and a strong positive peak at 1254 cm^{-1} is obtained. In both cases, the vibrational coupling is clearly determined by the large nearest-neighbor coupling constants of -7.5 and $-7.2\ cm^{-1}$, respectively. Again, one finds the regular coupling pattern discussed earlier, with the in-phase combination at lower wavenumbers and the out-of-phase combination at lower wavenumbers. For the α helix, the nearest-neighbor intensity coupling terms (see Figure 4e) are rather small, whereas the second- and third-nearest-neighbor coupling terms are larger and negative. As discussed for the amide II and the C^{α}–H bending (II) bands, this leads to an increased negative intensity for both the in-phase and the out-of-phase combinations and, therefore, to splitting into two negative peaks. In contrast, for the 3_{10}-helix, the nearest-neighbor coupling is negative and larger in magnitude than the second-nearest-neighbor one, which explains the observed couplet. However, the intensity coupling terms are for both helices comparably small, so that both the splitting and the couplet are not very pronounced.

Comparison with experimental spectra: To identify which features of experimental ROA spectra are reproduced correctly by our calculations and for which features an improved theoretical description that also takes microsolvation effects into account might be necessary, we compare the calculated ROA spectrum of α-helical Ala_{20} to available experimental spectra in the following. Since in solution such short alanine polypeptides do not adopt the idealized α-helical structure investigated here, but are instead frayed at the termini,[22] we compare to spectra measured for (all-*S*)-polyalanine. This procedure is in accord with our general philosophy that the helical polypeptides represent fragments of protein secondary structure and should therefore closely resemble the ideal helical motifs. Alanine polypeptides usually do not adopt a 3_{10}-helical conformation in solution, and only one experimental spectrum of a 3_{10}-helical heptapetide in aqueous solution is available in the literature.[60] However, this heptapetide consists of C^{α}-tetrasubsituted residues with rather complex side chains, which significantly alter the ROA spectrum with respect to the one that could be expected for peptides containing standard amino acids. Nevertheless, this is not a drawback, since a validation for the α-helical model should assure us of the ROA results for the 3_{10}-helical model, and make the latter a true prediction to be challenged by experiment.

In ref. [51], the positions of the bands in the calculated parent IR and Raman spectra of α-helical Ala_{20} were compared to those in the experimental spectra of solid (all-*S*)-polyalanine,[61,62] and a good agreement was found for all bands, with the largest deviations occurring for the amide II band and for the extended amide III region, in which the positions of the bands are underestimated by up to 30 cm^{-1}. For the other bands in the investigated wavenumber range, the differences were found to be smaller than 10 cm^{-1}. However, the structures of the polypeptides investigated in ref. [51] were closer to a 3_{10}-helix than to an α helix because it only contained 10 alanine residues and, therefore, some of the assignments were uncertain.

In Figure 5, the calculated ROA spectrum of α-helical Ala_{20} is shown together with the experimental solution spectra of (all-*S*)-polyalanine in dichloracetic acid (DCA) and in a mixture of 30% DCA and 70% chloroform. The spectra measured in the two different solvents are very similar; the only notable exceptions are the different relative intensities of the peaks at 1304 and 1338 cm^{-1}. Note that the weak negative peak at 1215 cm^{-1} in the spectrum in 30% DCA/70% CH_3Cl is related to the solvent.[28]

The couplet, negative at low wavenumbers and positive at high wavenumbers, found for the amide I band between

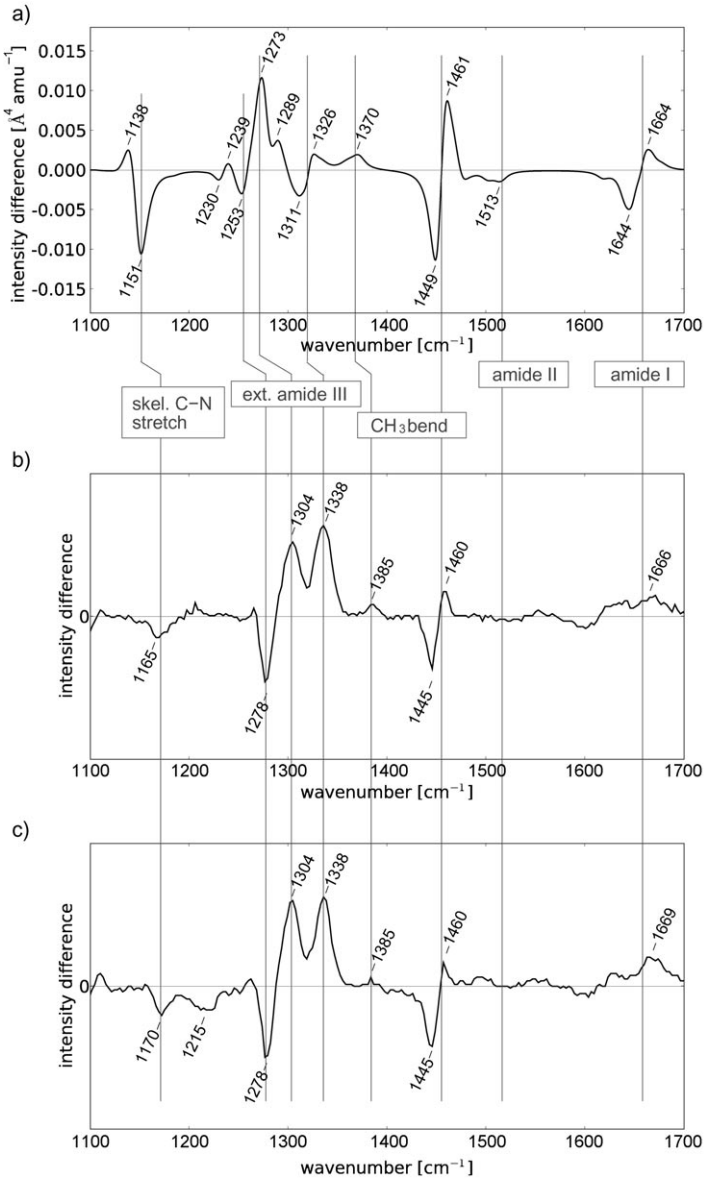

Figure 5. Comparison of a) the calculated ROA spectrum of α-helical Ala_{20} (no solvent effects) with experimental spectra measured for α-helical (all-*S*)-polyalanine in b) dichloracetic acid (DCA) and c) in 30% DCA/70% CH_3Cl. Experimental spectra have been taken from ref. [28].

1640 and 1670 cm^{-1} in our calculations is also observed in the experimental spectra, even though the negative part is very weak in the experimental (all-*S*)-polyalanine spectra. However, a more pronounced amide I couplet is observed in the experimental ROA spectra of other α-helical polypeptides and proteins, and has been identified earlier as a signature of α helices.[24] As in the calculated spectrum, the amide II band (between 1470 and 1520 cm^{-1}) is absent in the experimental ROA spectrum. Furthermore, the couplet centered at approximately 1455 cm^{-1} obtained for the asymmetric CH_3 bending band in the calculated ROA spectrum agrees very well with the couplet found in the experimental spectra at the same position. Similarly, the weak positive symmetric CH_3 bending found at 1370 cm^{-1} in the calculations agrees with the weak positive band found experimentally at 1385 cm^{-1}. Finally, also the negative peak observed experimentally at 1165–1170 cm^{-1} for the skeletal C^{α}–N stretching band is reproduced correctly by the calculations.

However, the agreement is not that good for the bands in the extended amide III region. According to our assignment, the positive peak at 1338 cm^{-1} in the experimental spectra corresponds to the C^{α}–H bending (I) band, for which a couplet, centered at approximately 1320 cm^{-1} is found in the calculated spectrum. The positive peak at 1304 cm^{-1} in the experimental spectra corresponds to the C^{α}–H bending (II) band, for which a strong positive peak at 1273 cm^{-1}, together with a somewhat weaker one at 1289 cm^{-1} is found in the calculated spectrum. The negative peak at 1278 cm^{-1} in the experimental spectra can be identified with the amide III band, for which a weak negative peak at 1253 cm^{-1} is obtained in the calculated spectrum. Although for the C^{α}–H bending (I) band, neither the band shape nor the total intensity obtained from the calculations agree with the experimental spectra, the calculated C^{α}–H bending (II) and amide III bands qualitatively agree with experimental results. However, the relative ROA intensities of the different peaks are also not described well in the calculations, since the amide III band at 1278 cm^{-1} is much stronger in the experimental spectra than in the calculated spectra.

The discrepancies between our calculations and experimental results for the bands in the extended amide III region can be understood in view of the analysis presented above. Both the localized modes and their ROA intensities as well the intensity coupling terms for the bands in the extended amide III region are very sensitive to the coupling between the classical amide III vibration and the C^{α}–H bending vibrations, which depends on the backbone structure and on the precise positions of these bands.[51] The position of the classical amide III vibration as well as its ROA intensity (and the associated coupling terms) is in turn very sensitive to solvent effects, as polar solvents form hydrogen bonds to the amide groups. Therefore, the coupling between the classical amide III and the C^{α}–H bending vibrations and thus also the resulting ROA spectra in the extended amide III region can be expected to be very sensitive to both the chosen structural model and the description of solvent effects.

An important experimental finding can be understood on the basis of our analysis. Even though the positions of the two C^{α}–H bending bands do not change significantly (less than 10 cm^{-1}) upon deuteration of the amide N–H groups[62] (since the contribution of the classical amide III vibration is small), the C^{α}–H bending (I) peak at around 1340 cm^{-1} in the ROA spectrum disappears.[28] The C^{α}–H bending (II) is also affected, but to a smaller extent. Upon deuteration, the classical amide III vibration shifts to lower wavenumbers so that it does not couple with the C^{α}–H bending vibrations any longer, (i.e., in the deuterated polypeptide, there is no contribution of the classical amide III vibration to the C^{α}–H bending bands). However, as shown above, the ROA intensity of the localized modes corresponding to the C^{α}–H bend-

ing bands is mainly due to this coupling with classical amide III vibration. Therefore, the ROA intensity of these bands significantly decreases upon deuteration.

Identifying signatures of the α helix and 3_{10}-helix: Although α-helical structures have been studied in detail using ROA spectroscopy and several signatures of α-helical structures have been identified,[28] only little is known about spectral signatures of 3_{10}-helices. An early assignment of a peak at around 1340 cm^{-1} to a 3_{10}-helix[63] had to be revised later.[24] By comparing the ROA spectra calculated for α-helical and for 3_{10}-helical Ala_{20}, it is possible to extract signatures that might be used to discriminate between α helix and 3_{10}-helix by means of ROA spectroscopy. Notable differences occur for the amide I and II bands, as well as for the bands in the extended amide III region. Although differences are also found for the asymmetric CH_3 bending band, this band is related to the alanine side chains and is not present in other amino acids, so that it is not generally useful.

In the amide I region, a couplet, which is negative at low and positive at high wavenumbers, is found for the α-helical Ala_{20}. Such a couplet has been identified earlier as a signature of α helices by comparing experimental spectra of polypeptides and proteins containing α-helical secondary-structure elements.[25,28] In contrast, the opposite couplet, positive at low and negative at high wavenumbers is found for the 3_{10}-helical Ala_{20}. Through the analysis presented above, these different couplets can be explained by the different vibrational coupling constants for the two conformers. These differences in the vibrational coupling are directly related to the backbone structure. Even though we have extracted these vibrational coupling constants from the calculations on the full systems, for the amide I band the different pattern can be qualitatively explained by a transition dipole coupling model.[50,64] For the α helix, amide C=O groups of nearest-neighboring residues are oriented in parallel, so that a large, positive nearest-neighbor coupling constant is obtained. For the 3_{10}-helix, the nearest-neighbor coupling constant is smaller, and the coupling with the vibration of the C=O group of the second-nearest-neighboring residue, which has a negative sign, is dominant. This can be understood, since for the 3_{10}-helix, this second-nearest-neighbor coupling corresponds to one complete turn of the helix, and the fact that the opposite couplet is obtained for the 3_{10}-helix is thus directly related to the different number of residues within one turn of the helix. Therefore, this amide I ROA couplet might be used to discriminate between α-helical and 3_{10}-helical structures. However, in proteins containing both α-helical and 3_{10}-helical secondary-structure elements, the different couplets might overlap and thus partly cancel, so that they could be difficult to distinguish.

A second signature can be identified for the amide II band. In the α helix calculation, the amide II band is not visible in the plotted spectra. This agrees with the experimental observation that the amide II band is absent in the ROA spectra of α-helical polypeptides and proteins.[25,28] In contrast, the amide II band appears in the calculated spectra of 3_{10}-helical Ala_{20}. We note that this agrees with the calculation of the Raman spectrum,[50] which also shows an increased intensity for the 3_{10}-helical structure. In both cases, the increased intensity can be traced back to increased intensities of the amide II localized modes that are due to changes in the electronic structure. Our calculations predict that the amide II band in 3_{10}-helices is split into two peaks. This splitting is due to the structure of the amide II intensity coupling matrix, in which the nearest-neighbor coupling terms are negligible, whereas the second-nearest-neighbor coupling terms are significantly larger in magnitude. These intensity coupling terms depend on the orientation of the different amide groups with respect to each other, so that this band shape can be directly related to the secondary structure.

Several differences between the calculated spectra of the two conformers are also found in the extended amide III region. In particular, the amide III band is negative in α-helical Ala_{20} and positive in 3_{10}-helical Ala_{20}. However, as our analysis shows, the total intensities of this band sensitively depend upon the degree of mixing between the classical amide III and the C^{α}–H bending vibrations.[51] This not only depends upon the secondary structure, but its accurate description might also require an adequate treatment of solvent effects.

Conclusion

To understand the generation of ROA signals in proteins and to gain insight into the relation between secondary structure and measured ROA spectra, we have analyzed the calculated ROA spectra of two large α-helical and 3_{10}-helical Ala_{20} polypeptides by transforming the normal modes contributing to each ROA band to rigorously defined localized modes. These localized modes are—in contrast to the delocalized normal modes—in general rather simple and each of them involves only vibrations of one residue, with localized modes on different residues being similar. It is then possible to explain the total band intensities in terms of the intensities of representative localized modes. Furthermore, the band shapes can be rationalized in terms of the vibrational coupling of the localized modes to normal modes and of the intensity coupling terms, which describe the contributions to the ROA intensities that are due to the coupling between localized modes. A number of conclusions can be extracted from this analysis, which will apply not only to the model systems studied here, but to the ROA spectra of polypeptides and proteins in general.

For the generation of the ROA intensities of the localized modes, which in turn determine the total band intensities, two different basic mechanisms can be distinguished. For the first class of bands, the ROA intensity of the localized modes is due to a single, achiral group of atoms. This is the case for the amide I band, the amide II band, and for the asymmetric and symmetric CH_3 bending bands. For these bands, the total band intensities are solely caused by the

"electronic chirality" (i.e., the chirality of the electronic structure is probed by a vibration of an achiral group).[33,65] For the second class of bands, the ROA intensity of the localized modes is due to the coupling between vibrations of two different groups. This is observed for the bands in the extended amide III region, in which the ROA intensity can be mainly attributed to the coupling between the C^{α}–H bending and the classical amide III vibration, and for the skeletal C^{α}–N stretching band. For these bands, the total intensities are mainly due to "vibrational chirality" (i.e., the arrangement of the vibrating atoms is chiral by itself).[19]

The localized-mode ROA intensities and thus also the total band intensities can be affected by secondary-structure changes in different ways. First, changes in the composition of the relevant localized modes induced by structural changes will affect the ROA intensities of these modes. This is particularly important for the bands in the extended amide III region, in which the degree of mixing between the C^{α}–H bending and the classical amide III vibrations sensitively depends upon the backbone dihedral angles.[51] For the two model systems studied here, these changes in the composition of the localized modes lead to a redistribution of ROA intensity between the C^{α}–H bending (II) and the amide III band. Second, in the cases in which the localized-mode ROA intensities are due to vibrational chirality (i.e., due to the coupling between vibrations of two different groups of atoms), the ROA intensity directly depends on the orientation of these two groups with respect to each other[19] and is, therefore, directly affected by structural changes. Third, structural changes imply changes in the electronic structure, which in turn affect the polarizability derivatives that determine the ROA intensity. This is the only mechanism that is relevant for the bands in which the ROA intensity of the localized modes is determined solely by the electronic chirality, since generally in these cases the localized modes themselves are not affected by structural changes.

The ROA band shapes are determined by the coupling between localized modes on different residues. Both the vibrational coupling constants, which describe the coupling of localized modes to normal modes, and the intensity coupling matrices, which determine the ROA intensities of these coupled modes, are directly related to the orientation of the different amino acid residues with respect to each other. Therefore, the ROA band shapes are a sensitive probe of the backbone structure. For the generation of the ROA band shapes, three important patterns can be distinguished. First, if either the vibrational coupling constants or the intensity coupling terms are small, a single peak is observed, and the intensity of this peak is determined by the intensities of the localized modes. This is, for instance, found for the symmetric CH_3 bending band. Second, if the nearest-neighbor intensity coupling terms are large, and if, in addition, the vibrational coupling is sufficiently large, a couplet is observed. Whether this couplet is positive at low and negative at high wavenumbers or the other way around depends on the sign of the nearest-neighbor intensity coupling terms and on the order of the coupled normal modes, which is in most cases determined by the sign of the largest vibrational coupling constant. A prototypical example of this is the amide I band, for which we showed that the inversion of the couplet for the α helix and for the 3_{10}-helix can be traced back to the different vibrational coupling constants. Third, if the nearest-neighbor intensity coupling terms are small and the second nearest-neighbor intensity coupling terms are large, the band splits into two peaks, as is, for instance, found for the amide II band in 3_{10}-helical Ala_{20}.

The analysis of the calculated ROA spectra presented here not only provides an understanding of the generation of ROA bands for the model systems considered, but it also enables us to predict which qualitative features of the spectra will be sensitive to insufficiencies of the computational methodology. In particular, the use of the harmonic approximation, the approximate exchange-correlation functional used in the DFT calculations, the neglect of solvent effects, and the particular choice of the structural models will all affect the calculated ROA spectra. Our decomposition of the calculated ROA spectra allows us to trace specific features of the calculated spectra back to localized modes and the coupling between them and thus makes it possible to estimate how these spectral features are affected by changes of the structural model, of the force field, or of the polarizability tensor derivatives.

Therefore, we are able to draw general conclusions from our calculations and deduce signatures of specific secondary-structure elements. We can confirm the amide I couplet, negative at low and positive at high wavenumbers, as a signature of α helices and we can further predict that the opposite amide I couplet could serve as a signature of 3_{10}-helices. Since we can directly relate the amide I couplet to the vibrational coupling constants, which change due to the different number of residues within one turn of the helix, we can be confident that these different couplets are not due to the particular choice of the model systems or of the chosen structural models, or are an artifact caused by the approximations applied in the calculations of the ROA spectra.

On the other hand, the calculations provide a basic understanding of the generation of the ROA bands in the extended amide III region, and, for instance, explain how these bands are affected by deuteration of the amide N–H groups. However, since the bands in the extended amide III region are very sensitive to the degree of mixing between the C^{α}–H bending and the classical amide III vibrations, it is difficult to extract general relations from our calculations. In particular, to understand what precisely determines the relative intensities of the positive ROA bands at approximately 1300 and 1340 cm^{-1} and the absence of one of these bands in some cases,[28] and to explain how these bands are affected by solvent effects, more detailed studies that consider a larger number of different backbone structures and include an explicit description of the solvent will be necessary.

Nevertheless, the analytical methods established here open up the possibility to obtain a more detailed picture of

the generation of ROA bands in proteins. By systematically investigating a larger number of model systems, it will be possible to deduce how the localized modes, their ROA intensities, and the couplings between them depend upon the secondary structure. This might allow for a parametrization of simple but accurate models for the prediction of protein ROA spectra. Finally, we emphasize that the methodology employed here is not limited to ROA spectroscopy, but that VCD spectra can be analyzed and rationalized in a similar way.

Computational Methods

The molecular structures of the α-helical and 3_{10}-helical alanine polypeptides considered here have been taken from ref. [51]. The optimizations of these structures were performed with the TURBOMOLE program package[66,67] employing density functional theory as described in refs. [50,51] using the BP86 exchange-correlation functional[68,69] and Ahlrichs' valence triple-zeta basis with one set of polarization functions (TZVP).[70,71]

The SNF program[72,73] was used to calculate the normal modes and vibrational frequencies, as well as the polarizability tensor derivatives required for the calculation of the ROA backscattering intensities by numerical differentiation. The analytic energy gradients, which are needed for the seminumerical calculation of the harmonic force field, were calculated with TURBOMOLE for distorted structures.[72,73] As has been shown previously, the unscaled harmonic BP86 frequencies generally agree satisfactorily with the fundamental frequencies experimentally observed in solution experiments due to a systematic error cancelation.[74–76]

The polarizability tensors required for the ROA intensities were calculated with time-dependent DFT by an extended version[77] of the ESCF program[78–81] in TURBOMOLE using the same exchange-correlation functional and basis set as for the structure optimization. Although the optimized structures (as well as the IR and Raman spectra) have been reported before,[51] we should emphasize that our extensive ROA calculations reported here were carried out in such a way that the force field was recomputed rather than taken from ref. [51].

It has been shown previously that the ROA intensity differences of organic molecules are not sensitive to the choice of the exchange-correlation functional.[47,82] To ensure gauge invariance, the velocity representation of the electric-dipole operator was employed for the $\beta(\boldsymbol{G}')^2$ invariant.[77] The ROA intensities were calculated for an excitation wavelength of 799 nm, and it was verified that this chosen wavelength is well away from any electronic absorption frequency of the considered molecules.

For each of the characteristic bands in the ROA spectra, the localized modes are obtained by determining the unitary transformation of the normal modes contributing to this band that leads to optimally localized modes.[50] This has been done according to the atomic-contribution criterion and using the Jacobi sweep method as described in ref. [50]. Both the localization of normal modes and the related analysis routines are implemented in an add-on package to SNF. Details on the theoretical methodology employed for the calculation of the ROA intensities, on the determination of the localized modes, and on the analysis of the total band intensities and of the band shapes in terms of localized modes can be found in the Supporting Information.

Pictures of molecular structures and normal modes were prepared with JMOL.[83] Plots of vibrational spectra and of group- and intensity-coupling matrices were produced using the MATPLOTLIB package.[84] In the graphical representations of these coupling matrices, the area of the circles is proportional to the size of the corresponding matrix element, and filled circles represent positive, whereas empty circles represent negative contributions. Note that for these symmetric matrices only the upper triangular part is shown, and the off-diagonal matrix elements have, therefore, been multiplied by two.

Acknowledgements

C.R.J. acknowledges funding through a Rubicon scholarship of the Netherlands Organization for Scientific Research (NWO). This work has been supported by the Swiss National Science Foundation (SNF; project 200020-121870).

[1] D. Röthlisberger, O. Khersonsky, A. M. Wollacott, L. Jiang, J. DeChancie, J. Betker, J. L. Gallaher, E. A. Althoff, A. Zanghellini, O. Dym, S. Albeck, K. N. Houk, D. S. Tawfik, D. Baker, *Nature* **2008**, *453*, 190–195.

[2] L. Jiang, E. A. Althoff, F. R. Clemente, L. Doyle, D. Röthlisberger, A. Zanghellini, J. L. Gallaher, J. L. Betker, F. Tanaka, C. F. Barbas, D. Hilvert, K. N. Houk, B. L. Stoddard, D. Baker, *Science* **2008**, *319*, 1387–1391.

[3] K. Wüthrich, *NMR of Proteins and Nucleic Acids*, Wiley-Interscience, New York, **1986**.

[4] Z. Ganim, H. S. Chung, A. W. Smith, L. P. DeFlores, K. C. Jones, A. Tokmakoff, *Acc. Chem. Res.* **2008**, *41*, 432–441.

[5] W. Zhuang, T. Hayashi, S. Mukamel, *Angew. Chem.* **2009**, *121*, 3804–3838; *Angew. Chem. Int. Ed.* **2009**, *48*, 3750–3781.

[6] P. R. Carey, *J. Biol. Chem.* **1999**, *274*, 26625–26628.

[7] G. J. Thomas, Jr., *Biopolymers* **2002**, *67*, 214–225.

[8] E. Vass, M. Hollosi, F. Besson, R. Buchet, *Chem. Rev.* **2003**, *103*, 1917–1954.

[9] P. Hamm, M. Lim, R. M. Hochstrasser, *J. Phys. Chem. B* **1998**, *102*, 6123–6138.

[10] H. Maekawa, C. Toniolo, A. Moretto, Q. B. Broxterman, N.-H. Ge, *J. Phys. Chem. B* **2006**, *110*, 5834–5837.

[11] L. P. DeFlores, Z. Ganim, R. A. Nicodemus, A. Tokmakoff, *J. Am. Chem. Soc.* **2009**, *131*, 3385–3391.

[12] H. Maekawa, M. De Poli, C. Toniolo, N.-H. Ge, *J. Am. Chem. Soc.* **2009**, *131*, 2042–2043.

[13] R. Schweitzer-Stenner, *J. Raman Spectrosc.* **2001**, *32*, 711–732.

[14] A. Cua, D. H. Stewart, M. J. Reifler, G. W. Brudvig, D. F. Bocian, *J. Am. Chem. Soc.* **2000**, *122*, 2069–2077.

[15] A. V. Mikhonin, Z. Ahmed, A. Ianoul, S. A. Asher, *J. Phys. Chem. B* **2004**, *108*, 19020–19028.

[16] I. R. Rodriguez-Mendieta, G. R. Spence, C. Gell, S. E. Radford, D. A. Smith, *Biochemistry* **2005**, *44*, 3306–3315.

[17] C.-Y. Huang, G. Balakrishnan, T. G. Spiro, *J. Raman Spectrosc.* **2006**, *37*, 277–282.

[18] T. A. Keiderling, in *Circular Dichroism: Principles and Applications*, 2nd ed. (Eds.: N. Berova, K. Nakanishi, R. W. Woody), Wiley-VCH, New York, **2000**, pp. 621–666.

[19] L. D. Barron, *Molecular Light Scattering and Optical Activity*, 2nd ed., Cambridge University Press, Cambridge, **2004**.

[20] L. D. Barron, M. P. Bogaard, A. D. Buckingham, *J. Am. Chem. Soc.* **1973**, *95*, 603–605.

[21] W. Hug, S. Kint, G. F. Bailey, J. R. Scherer, *J. Am. Chem. Soc.* **1975**, *97*, 5589–5590.

[22] R. A. G. D. Silva, J. Kubelka, P. Bour, S. M. Decatur, T. A. Keiderling, *Proc. Natl. Acad. Sci. USA* **2000**, *97*, 8318–8323.

[23] J. Kubelka, R. A. G. D. Silva, T. A. Keiderling, *J. Am. Chem. Soc.* **2002**, *124*, 5325–5332.

[24] L. D. Barron, L. Hecht, E. W. Blanch, A. F. Bell, *Prog. Biophys. Mol. Biol.* **2000**, *73*, 1–49.

[25] L. D. Barron, E. W. Blanch, L. Hecht in *Advances in Protein Chemistry, Vol. 62* (Ed.: G. D. Rose), Elsevier, San Diego, **2002**, pp. 51–90.

[26] L. D. Barron, L. Hecht, I. H. McColl, E. W. Blanch, *Mol. Phys.* **2004**, *102*, 731–744.

[27] F. Zhu, N. W. Isaacs, L. Hecht, G. E. Tranter, L. D. Barron, *Chirality* **2006**, *18*, 103–115.

[28] I. H. McColl, E. W. Blanch, L. Hecht, L. D. Barron, *J. Am. Chem. Soc.* **2004**, *126*, 8181–8188.

[29] I. H. McColl, E. W. Blanch, A. C. Gill, A. G. O. Rhie, M. A. Ritchie, L. Hecht, K. Nielsen, L. D. Barron, *J. Am. Chem. Soc.* **2003**, *125*, 10019–10026.
[30] I. H. McColl, E. W. Blanch, L. Hecht, N. R. Kallenbach, L. D. Barron, *J. Am. Chem. Soc.* **2004**, *126*, 5076–5077.
[31] J. Kapitán, V. Baumruk, P. Bouř, *J. Am. Chem. Soc.* **2006**, *128*, 2438–2443.
[32] E. W. Blanch, L. Hecht, L. A. Day, D. M. Pederson, L. D. Barron, *J. Am. Chem. Soc.* **2001**, *123*, 4863–4864.
[33] Ch. R. Jacob, S. Luber, M. Reiher, *ChemPhysChem* **2008**, *9*, 2177–2180.
[34] F. Zhu, G. E. Tranter, N. W. Isaacs, L. Hecht, L. D. Barron, *J. Mol. Biol.* **2006**, *363*, 19–26.
[35] F. Zhu, J. Kapitan, G. E. Tranter, P. D. A. Pudney, N. W. Isaacs, L. Hecht, L. D. Barron, *Proteins Struct. Funct. Bioinf.* **2008**, *70*, 823–833.
[36] M. Pecul, K. Ruud, *Int. J. Quantum Chem.* **2005**, *104*, 816–829.
[37] C. Herrmann, M. Reiher, *Top. Curr. Chem.* **2007**, *268*, 85–132.
[38] J. Costante, L. Hecht, P. L. Polavarapu, A. Collet, L. D. Barron, *Angew. Chem.* **1997**, *109*, 917–919; *Angew. Chem. Int. Ed. Engl.* **1997**, *36*, 885–887.
[39] P. L. Polavarapu, *Angew. Chem.* **2002**, *114*, 4726–4728; *Angew. Chem. Int. Ed.* **2002**, *41*, 4544–4546.
[40] J. Haesler, I. Schindelholz, E. Riguet, C. G. Bochet, W. Hug, *Nature* **2007**, *446*, 526–529.
[41] C. Herrmann, K. Ruud, M. Reiher, *ChemPhysChem* **2006**, *7*, 2189–2196.
[42] P. Bouř, J. Sopková, L. Bednárová, P. Maloň, T. A. Keiderling, *J. Comput. Chem.* **1997**, *18*, 646–659.
[43] J. Kapitán, F. Zhu, L. Hecht, J. Gardiner, D. Seebach, L. D. Barron, *Angew. Chem.* **2008**, *120*, 6492–6494; *Angew. Chem. Int. Ed.* **2008**, *47*, 6392–6394.
[44] W. Hug, *Chem. Phys.* **2001**, *264*, 53–69.
[45] G. Zuber, W. Hug, *Helv. Chim. Acta* **2004**, *87*, 2208–2234.
[46] C. Herrmann, K. Ruud, M. Reiher, *Chem. Phys.* **2008**, *343*, 200–209.
[47] S. Luber, C. Herrmann, M. Reiher, *J. Phys. Chem. B* **2008**, *112*, 2218–2232.
[48] E. Lamparska, V. Liègeois, O. Quinet, B. Champagne, *ChemPhysChem* **2006**, *7*, 2366–2376.
[49] V. Liégeois, B. Champagne, *J. Comput. Chem.* **2009**, *30*, 1261–1278.
[50] Ch. R. Jacob, M. Reiher, *J. Chem. Phys.* **2009**, *130*, 084106.
[51] Ch. R. Jacob, S. Luber, M. Reiher, *J. Phys. Chem. B* **2009**, *113*, 6558–6573.
[52] E. B. Wilson, J. C. Decius, P. C. Cross, *Molecular Vibrations: The Theory of Infrared and Raman Vibrational Spectra*, Dover Publications, New York, **1980**.
[53] D. A. Long, *The Raman Effect: A Unified Treatment of the Theory of Raman Scattering by Molecules*, Wiley, New York, **2001**.
[54] J. Kubelka, R. Huang, T. A. Keiderling, *J. Phys. Chem. B* **2005**, *109*, 8231–8243.
[55] J. Neugebauer, M. J. Louwerse, E. J. Baerends, T. A. Wesolowski, *J. Chem. Phys.* **2005**, *122*, 094115.
[56] J. Neugebauer, C. R. Jacob, T. A. Wesolowski, E. J. Baerends, *J. Phys. Chem. A* **2005**, *109*, 7805–7814.
[57] C. R. Jacob, J. Neugebauer, L. Jensen, L. Visscher, *Phys. Chem. Chem. Phys.* **2006**, *8*, 2349–2359.
[58] M. Diem, *Introduction to Modern Vibrational Spectroscopy*, Wiley-Interscience, New York, **1993**.
[59] S. A. Overman, G. J. Thomas, Jr., *Biochemistry* **1998**, *37*, 5654–5665.
[60] C. Toniolo, F. Formaggio, S. Tognon, Q. B. Broxterman, B. Kaptein, R. Huang, V. Setnicka, T. A. Keiderling, I. H. McColl, L. Hecht, L. D. Barron, *Biopolymers* **2004**, *75*, 32–45.
[61] S. Krimm, J. Bandekar, *Adv. Protein Chem.* **1986**, *38*, 181–364.
[62] S.-H. Lee, S. Krimm, *Biopolymers* **1998**, *46*, 283–317.
[63] J. Teraoka, A. F. Bell, L. Hecht, L. D. Barron, *J. Raman Spectrosc.* **1998**, *29*, 67–71.
[64] W. H. Moore, S. Krimm, *Proc. Natl. Acad. Sci. USA* **1975**, *72*, 4933–4935.
[65] L. D. Barron, *J. Chem. Soc. A* **1971**, 2899–2904.
[66] TURBOMOLE, R. Ahlrichs et al., http://www.turbomole.com.
[67] R. Ahlrichs, M. Bär, M. Häser, H. Horn, C. Kölmel, *Chem. Phys. Lett.* **1989**, *162*, 165–169.
[68] A. D. Becke, *Phys. Rev. A* **1988**, *38*, 3098–3100.
[69] J. P. Perdew, *Phys. Rev. B* **1986**, *33*, 8822–8824.
[70] A. Schäfer, C. Huber, R. Ahlrichs, *J. Chem. Phys.* **1994**, *100*, 5829–5835.
[71] TURBOMOLE basis set library, ftp://ftp.chemie.uni-karlsruhe.de/pub/basen.
[72] J. Neugebauer, M. Reiher, C. Kind, B. A. Hess, *J. Comput. Chem.* **2002**, *23*, 895–910.
[73] SNF 4.0—A program for the quantum chemical calculation of vibrational spectra, J. Neugebauer, C. Herrmann, S. Luber, M. Reiher, http://www.reiher.ethz.ch/software/snf.
[74] G. Brehm, M. Reiher, S. Schneider, *J. Phys. Chem. A* **2002**, *106*, 12024–12034.
[75] M. Reiher, G. Brehm, S. Schneider, *J. Phys. Chem. A* **2004**, *108*, 734–742.
[76] G. Brehm, M. Reiher, B. Le Guennic, M. Leibold, S. Schindler, F. W. Heinemann, S. Schneider, *J. Raman Spectrosc.* **2006**, *37*, 108–122.
[77] S. Luber, M. Reiher, *Chem. Phys.* **2008**, *346*, 212–223.
[78] R. Bauernschmitt, R. Ahlrichs, *Chem. Phys. Lett.* **1996**, *256*, 454–464.
[79] R. Bauernschmitt, M. Häser, O. Treutler, R. Ahlrichs, *Chem. Phys. Lett.* **1997**, *264*, 573–578.
[80] F. Furche, R. Ahlrichs, *J. Chem. Phys.* **2002**, *117*, 7433–7447.
[81] S. Grimme, F. Furche, R. Ahlrichs, *Chem. Phys. Lett.* **2002**, *361*, 321–328.
[82] M. Reiher, V. Liégeois, K. Ruud, *J. Phys. Chem. A* **2005**, *109*, 7567–7574.
[83] JMOL—An open-source molecule viewer, http://jmol.sourceforge.net.
[84] MATHPLOTLIB—A Python 2D plotting library, http://matplotlib.sourceforge.net/.

Received: July 2, 2009
Published online: November 11, 2009

